

Article

The Cracking Resistance Behavior of Geosynthetics-Reinforced Asphalt Concrete under Lower Temperatures Using Bending Test

Qiaoyi Li ^{1,2} , Yonghai He ³, Guangqing Yang ^{1,4,*}, Penghui Su ^{1,2} and Biao Li ⁵

¹ State Key Laboratory of Mechanical Behavior and System Safety of Traffic Engineering Structures, Shijiazhuang Tiedao University, Shijiazhuang 050043, China; liqiaoyi@stdu.edu.cn (Q.L.); suphsph@163.com (P.S.)

² School of Traffic and Transportation, Shijiazhuang Tiedao University, Shijiazhuang 050043, China

³ Hebei Provincial Communications Planning, Design and Research Institute Co., Ltd., Shijiazhuang 050043, China; yonghaihe@126.com

⁴ School of Civil Engineering, Shijiazhuang Tiedao University, Shijiazhuang 050043, China

⁵ School of Management, Shijiazhuang Tiedao University, Shijiazhuang 050043, China; libiao_hb1990@163.com

* Correspondence: yanggq@stdu.edu.cn

Abstract: Asphalt is a kind of temperature-sensitive material. With the decrease of temperature, the deformation capacity of an asphalt mixture will be significantly reduced. When the temperature is greatly reduced, the asphalt layer will produce large shrinkage tensile stress and strain, resulting in cracking. Therefore, the cracking resistance behavior is essential for the asphalt. In order to study the cracking resistance behavior of geosynthetics-reinforced asphalt under lower temperatures, the bending tests were carried out indoors at a temperature of $-10\text{ }^{\circ}\text{C}$. The results showed that compared with the unreinforced asphalt sample, the flexural tensile strength at failure of the geogrid-reinforced sample was increased by 14.1% and 12.3%, corresponding to AC-13C and AC-20C. Additionally, the geotextile-reinforced sample was reduced by 2.5% and 3.6%, corresponding to AC-13C and AC-20C. The values of the bending stiffness modulus of the geogrid- and geotextile-reinforced samples were reduced by 6% and 1%. The cracking energy of the geogrid-reinforced asphalt provides by 45.2% and 30.8% more than unreinforced asphalt, corresponding to AC-13C and AC-20C. The cracking energy of the geotextile-reinforced asphalt is increased by 4.5% and 0.6% compared with unreinforced asphalt, corresponding to AC-13C and AC-20C. The cracking resistance behavior of geogrid-reinforced asphalt is better than unreinforced and geotextile-reinforced asphalt. The asphalt shows obvious brittleness at a temperature of $-10\text{ }^{\circ}\text{C}$, and the existence of the geosynthetics does not change the shape of the load–deflection curves.

Keywords: geosynthetics; geogrid; geotextile; reinforcement; asphalt concrete; the bending test



Citation: Li, Q.; He, Y.; Yang, G.; Su, P.; Li, B. The Cracking Resistance Behavior of Geosynthetics-Reinforced Asphalt Concrete under Lower Temperatures Using Bending Test. *Coatings* **2022**, *12*, 812. <https://doi.org/10.3390/coatings12060812>

Academic Editors: Ofelia-Cornelia Corbu and Ionut Ovidiu Toma

Received: 7 May 2022

Accepted: 8 June 2022

Published: 10 June 2022

Publisher's Note: MDPI stays neutral with regard to jurisdictional claims in published maps and institutional affiliations.



Copyright: © 2022 by the authors. Licensee MDPI, Basel, Switzerland. This article is an open access article distributed under the terms and conditions of the Creative Commons Attribution (CC BY) license (<https://creativecommons.org/licenses/by/4.0/>).

1. Introduction

Geosynthetics-reinforced asphalt has attracted much focus in recent years. Geosynthetics in asphalt can effectively improve fatigue life and decrease rutting [1–6]. Meanwhile, it also can improve the cracking resistance of the asphalt. There are many studies on the cracking resistance of geosynthetics-reinforced asphalt. Canestrari et al. [7] carried out a three-point bending test at a temperature of $20\text{ }^{\circ}\text{C}$ on a geogrid-reinforced asphalt beam. Results show that the reinforced interfaces lead to higher peak load and deflection values. Zofka et al. [8] also conducted a three-point bending test on three kinds of different asphalt beams at a temperature of $13\text{ }^{\circ}\text{C}$. He pointed out that four times more energy is necessary for the crack to propagate through the carbon-reinforced beam than the unreinforced beam. The effect of reinforcement, in particular the CF geogrid, is significant. Ingrassia et al. [9] studied the cracking resistance of two geomembranes-reinforced asphalts and one geogrid-reinforced asphalt compared with unreinforced asphalt at $20\text{ }^{\circ}\text{C}$. Results show that the

unreinforced system exhibits a higher value of flexural strength (P_{max}) than the reinforced systems. However, after reaching P_{max} , unreinforced asphalt rapidly loses its resistance until complete failure, without any residual flexural resistance. On the contrary, the reinforced systems show a significant post-peak dissipative phase. The geocomposites increased the energy necessary for the crack propagation by three to eight times compared to the unreinforced pavement. Ragni et al. [10] assessed the effectiveness of asphalt pavement rehabilitation with geocomposites to limit fatigue cracking, reflective cracking, and rutting. Kumar et al. [11] evaluated the cracking resistance potential of geosynthetic-reinforced asphalt overlays by using a direct tensile strength test at 20, 30, and 40 °C. He pointed out that the performance of specimens conditioned at temperatures of 20 °C is superior to those at 30 and 40 °C. Spadoni et al. [12] assessed the influence of four different geocomposites, obtained by combining a reinforcing geosynthetic with a bituminous membrane, regarding the crack propagation and interlayer bonding of asphalt pavements. The three-point bending test was carried out on double-layered asphalt specimens at temperatures of 20 °C. Results showed that the main contribution of the geocomposites consisted in increasing the crack propagation energy in the layer above the reinforcement (from five to ten times with respect to the unreinforced system). Ram Kumar et al. [13] reviewed the flexural fatigue properties, interfacial shear characteristics, and mechanical properties of geogrids embedded with asphalt layers. From their summary and the literature reviewed, it can be summarized that many scholars mainly research the cracking resistance of the geosynthetics-reinforced asphalt at a temperature of 20 °C. There are few studies on the cracking resistance of the geosynthetics-reinforced asphalt under lower temperatures.

In this paper, the objective of this study was to investigate the cracking resistance of reinforced asphalt and unreinforced asphalt at a temperature of −10 °C. The obtained results were then compared with previously published results to obtain a more comprehensive understanding of the geosynthetics-reinforced asphalt.

2. Materials and Methods

2.1. Geosynthetics

In this study, geogrids and geotextiles were used in asphalt reinforcement. The transverse ribs coated with bitumen of the geogrid were made of 12K carbon fiber, the longitudinal ribs made of 1100 Tex glass fiber, and the geotextile were made of polyester fiber. Table 1 shows the properties of the geosynthetics used in this study.

Table 1. Characteristics of geosynthetics.

Geosynthetic	Direction	Material	Thickness (mm)	Elongation at Rupture (%)	Tensile Force (kN/m)
Geotextile	Longitudinal	Polyester glass fiber	1.2	4.6	9.40
	Transversal	Polyester glass fiber	1.2	4.7	9.28
Geogrid	Longitudinal	Glass fiber	0.7	3–4.5	45.00
	Transversal	Carbon fiber	0.7	2–2.5	76.92

2.2. Asphalt Mix Design

There were two kinds of double-layered hot-mix asphalt slab specimens made in the study. One double-layered asphalt was made of the AC-20C asphalt mixture. The AC-20C asphalt mixture was composed of crushed limestone aggregates and 4.3% bitumen content by weight. The aggregates were divided into 5 specifications: 16–22 mm limestone aggregate, 11–16 mm limestone aggregate, 6–11 mm limestone aggregate, 3–6 mm limestone aggregate, and 0–3 (machine-made sand) limestone aggregate. The density of the aggregates is shown in Table 2. The nominal maximum size of the AC-20C asphalt mixture was 22 mm. Another double-layered asphalt was made of two asphalt mixtures, AC-13C and AC-20C. The lower layer consisted of AC-20C, the same as the first type of asphalt, and the upper layer was an AC-13C asphalt mixture. The AC-13C asphalt mixture was composed of

crushed limestone aggregates and 4.8% bitumen content by weight. The nominal maximum size of the AC-13C asphalt mixture was 15 mm. The asphalt mix design was based on JTGF40-2004. The mineral aggregate gradation of asphalt mixture is presented in Table 3. Before fabrication of reinforced beam sample, asphalt mixture density test and Marshall stability test was conducted indoors according to the JTG E20-2011. The property of the asphalt was shown in Table 4. The bitumen was SBS-modified bitumen, penetration in 25 °C (0.1 mm) of 55, softening point of 81 °C, flashpoint of 270 °C, and Brookfield viscosity 135 °C of 1.9 Pa/s.

Table 2. The density of the aggregates.

Size	Bulk Density(g/cm ³)	Apparent Specific Gravity
16–22 mm	2.680	2.745
11–16 mm	2.687	2.743
6–11 mm	2.681	2.748
3–6 mm	2.683	2.747
0–3 mm (machine-made sand)	2.617	2.737

Table 3. Mineral aggregate gradation of asphalt mixture.

Sieve Size (mm)	AC-13C	AC-20C
	Passing (%)	Passing (%)
26.5	-	100.0
19	-	99.5
16	100.0	90.5
13.2	98.1	75.9
9.5	76.8	61.0
4.75	50.8	40.5
2.36	36.4	30.0
1.18	26.8	22.0
0.6	17.2	14.1
0.3	11.8	9.6
0.15	8.3	6.6
0.075	6.3	5.0

Table 4. The property of the asphalt.

-	Void Ratio/%	Aggregate Clearance Rate/%	Asphalt Saturation/%	Stability/kN	Flow Value/mm	Marshall Modulus (kN/mm)
AC-13C	3.1	11.0	77.2	14.2	3.6	3.944
AC-20C	3.5	14.2	75.0	14.4	3.4	4.364

2.3. Sample Production

The preparation process of geosynthetics-reinforced asphalt trabecular specimen mainly includes five processes: asphalt mixture production, lower-layer rolling forming, laying geosynthetics, upper-layer rolling forming, and plate cutting. Asphalt mixture production: The dried mineral aggregate and bitumen mixed to homogenous in the asphalt mixture mixer. Lower-layer rolling forming: The homogenous asphalt mix was put into the mold of 300 mm × 300 mm × 50 mm size. Compaction carried out by a roller to form a base plate. Laying geosynthetics: When lower-asphalt slab cooled to approx. 25 °C, placed the lower slab to mold (300 mm × 300 mm × 100 mm), and brushed the tack coat on the surface of the plate before the installation of geogrid. The tack coat was painted at 0.5 L/m². Plate cutting: Five beams were cut from the double-layered asphalt slab. The dimension of beam sample was L/H/W = 250/50/47 (unit: mm). The preparation of the test specimen is presented in Figure 1.



Figure 1. The preparation of test specimens. (a) Asphalt-mixture mixing; (b) layer rolling forming; (c) laying geosynthetics and brushing the tack coat; (d) double-layered asphalt slab; (e) plate cutting; (f) beam sample of the bending test.

2.4. Bending Tests

Before the bending test, the beam samples must be placed in a low temperature environment of $-10\text{ }^{\circ}\text{C}$ for no less than 4 h. The bending test was carried out at an ambient temperature of $-10\text{ }^{\circ}\text{C}$. The loading rate was 50.8 mm/min . Many research projects used this displacement rate [7–10]. When the load value reached 60% of the maximum load, the beam sample was considered to be damaged and the test ended. The bending test apparatus is shown in Figure 2. Five repetitions were performed for each test condition.

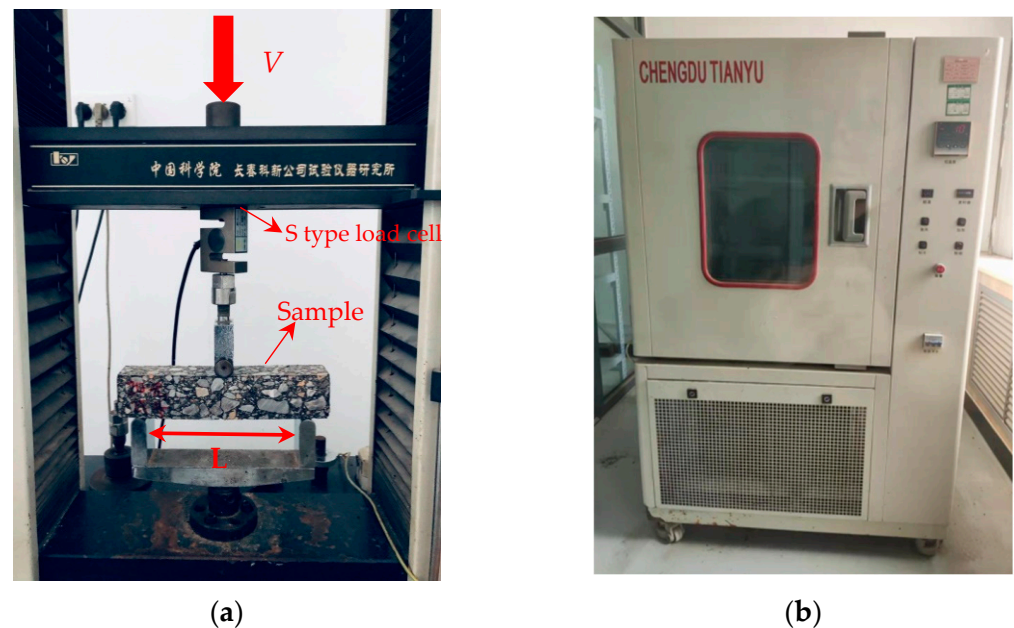


Figure 2. Test apparatuses. (a) The bending test apparatus; (b) temperature control box. Chinese in the figure: Changchun Kexin Company Test Instrument Research Institute, Chinese Academy of Sciences, Changchun, China.

The flexural strength point (P_{\max} , $\delta_{P,\max}$) was obtained by the bending test. It is noticed that when the difference between a certain data in a group of measured values and the average value is greater than 1.67 times of the standard deviation, the measured value shall be discarded (JTG E20-2011) and the average value of other measured values shall be taken as the test result. The values of R_B , ϵ_B , and S_B can be calculated from the following Equations:

$$R_B = \frac{3 \times L \times P_{\max}}{2 \times b \times h} \quad (1)$$

$$\epsilon_B = \frac{6 \times h \times \delta}{L^2} \quad (2)$$

$$S_B = \frac{R_B}{\epsilon_B} \quad (3)$$

R_B —Flexural tensile strength of specimen at failure, MPa.

ϵ_B —Maximum bending tensile strain of specimen at failure, $\mu\epsilon$.

S_B —Bending stiffness modulus of specimen at failure, MPa.

b —Mid-span width of specimen, mm.

h —Mid-span height of specimen, mm.

L —The span length of specimen, mm.

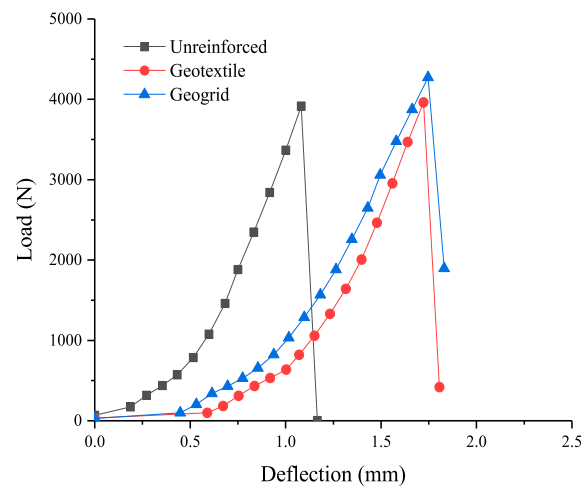
P_{\max} —Maximum load of specimen, N.

δ —Mid-span deflection of specimen in failure, mm.

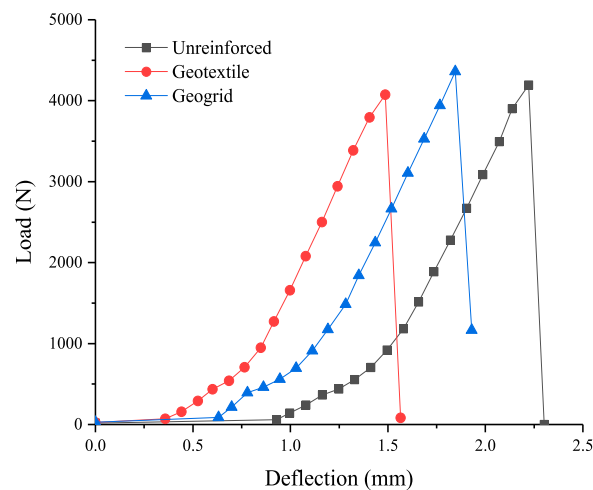
3. Results and Discussion

3.1. The Bending Test Results

The load–deflection curves obtained in the bending test are reported in Figure 3 and the average values of the corresponding characteristic parameters are summarized in Table 5.



(a)



(b)

Figure 3. The load vs. deflection curves. (a) AC-13C and (b) AC-20C.

Table 5. The average values of the corresponding characteristic parameters.

Asphalt Mix	Interface Type	P_{max} (N)	δ (mm)	R_B (MPa)	ϵ_B ($\mu\epsilon$)	S_B (MPa)
AC-13C	Unreinforced	3780.45	0.72	9.65	5381.250	1793.67
	Geotextile	3683.78	0.73	9.41	5484.375	1714.94
	Geogrid	4311.11	0.87	11.01	6528.075	1686.12
AC-20C	Unreinforced	4012.11	0.80	10.24	6034.200	1697.60
	Geotextile	3865.55	0.75	9.87	5608.475	1759.75
	Geogrid	4504.67	0.91	11.50	6853.325	1678.02

Table 5 shows that the order of the flexural tensile strength R_B value from large to small was $R_B^{CF} > R_B^{UN} > R_B^{GT}$. Compared with the flexural tensile strength R_B^{UN} of the unreinforced asphalt sample, the value of the flexural tensile strength R_B^{CF} of the geogrid-reinforced sample was increased by 14.1%, and the value of the flexural tensile strength R_B^{GT} of the geotextile-reinforced asphalt sample was reduced by 2.5%, corresponding to AC-13C. For the AC-20C, the value of the flexural tensile strength R_B^{CF} of the geogrid-reinforced sample was increased by 12.3%; the value of the flexural tensile strength R_B^{GT} of

the geotextile-reinforced asphalt sample was reduced by 3.6%. The order of the maximum bending tensile strain value at failure was $\varepsilon_B^{CF} > \varepsilon_B^{UN} > \varepsilon_B^{GT}$, corresponding to AC-20C. However, for the AC-13C, the order is $\varepsilon_B^{CF} > \varepsilon_B^{GT} > \varepsilon_B^{UN}$. This indicated that the geogrid can effectively improve the maximum bending tensile strain and alleviate the brittleness of asphalt at lower temperatures. When the cracks develop from the bottom of the asphalt beam to the interface, due to the network structure of the geogrid, the expansion of the cracks will be limited, and it is reflected in the test results that the asphalt beam shows a high tensile strain.

The order of the bending stiffness modulus value at failure was $S_B^{UN} > S_B^{GT} > S_B^{CF}$, corresponding to AC-13C. Compared with the bending stiffness modulus value S_B^{UN} of the unreinforced asphalt sample, the values of the bending stiffness modulus S_B^{CF} , S_B^{GT} were reduced by 6% and 1%, respectively, for the geogrid-reinforced asphalt and geotextile-reinforced asphalt. However, for the AC-20C, the order of the bending stiffness modulus value at failure was $S_B^{GT} > S_B^{UN} > S_B^{CF}$. It indicated that the geogrid is beneficial to improve the stress relaxation performance of asphalt, so as to inhibit the generation of cracks and prolong the failure time, and improve the low-temperature crack resistance of asphalt.

The stress is transferred through the mineral aggregate particles, and the geogrid laid on the interface of the asphalt mixture layer is equivalent to forming a “stress absorption layer”, which changes the transfer mode of the interlayer force. In the process of stress transfer from top to bottom, part of the stress is dissipated when it is transferred to the “stress absorption layer”, so that the remaining stress can be uniformly transferred to the bottom, thus delaying the generation of cracks. When the tensile stress at the bottom of the specimen exceeds the ultimate tensile strength of the asphalt mixture, cracks will occur at the bottom of the specimen and expand rapidly. When the crack extends to the geosynthetics, the presence of geosynthetics changes the stress at the crack tip, effectively reduces the stress concentration phenomenon, and is conducive to preventing the extension of the crack. At the same time, the tensile force, interlayer adhesion, and the friction of geosynthetics will restrict the opening deformation of cracks [7–9,13].

From the flexural tensile strength and strain to the flexural tensile strength and the bending stiffness modulus, the geogrid-reinforced asphalts have a better behavior on the cracking resistance under lower temperature. Figure 3 shows that the load–deflection curves are smooth in the whole test process and that the existence of the geosynthetics does not change the shape of the curve. For the AC-13C, the initial deflections of the geogrid and geotextile asphalt layer are higher than the unreinforced sample. However, the initial deflections of the geogrid and geotextile asphalt layer are lower than the unreinforced sample for the AC-20C.

3.2. Comparative Analysis with Previous Studies

Figure 4 shows the load–deflection curves obtained by other scholars. All results show that reinforcement has no effect on crack initiation at a temperature of 20 or 13 °C. There is, however, a significant impact on the softening region; that is, geosynthetics decrease the crack propagation after the crack has been initiated. Compared to the previously published results at a temperature of 20 or 13 °C (Figure 4), with the results at a temperature of −10 °C in this paper (Figure 3), we found that when the load reached the maximum value, the transformation trend of load deflection curve will be different. At the temperature of −10 °C, the crack developed to the top, and the double-layer asphalt beam was destroyed rapidly. However, at a temperature of 20 or 13 °C, the geogrid decreases the crack propagation. It shows that in a low-temperature environment, the effect of a geogrid on crack development is weaker than that in normal temperature environment. The flexural tensile strain of asphalt at a temperature of −10 °C is lower, the thickness of the upper asphalt is thin, and the beam is damaged too fast.

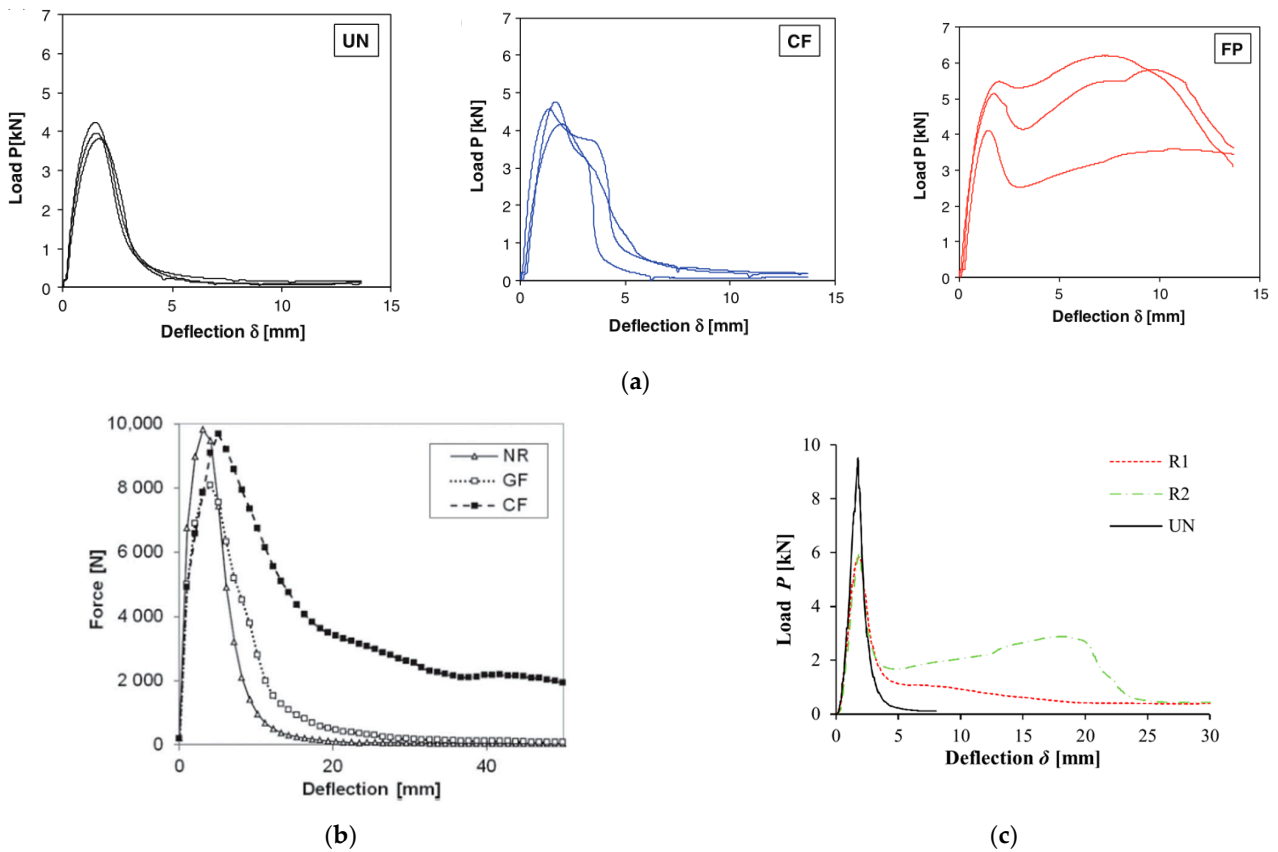


Figure 4. The load–deflection curves obtained by other scholars. (a) Reprinted with permission from [7]; Copyright 2013 Springer Nature; (b) Reprinted with permission from [8]; Copyright 2018 Taylor & Francis; (c) Reprinted with permission from [9].

Figure 5 shows the cracking energy of the six types of asphalt samples. The cracking energy of the geogrid-reinforced asphalt beam is higher than the unreinforced and geotextile-reinforced asphalt beam. The cracking energy of the geogrid-reinforced asphalt is 45.2% and 30.8% higher than unreinforced asphalt, corresponding to AC-13C and AC-20C. The cracking energy of the geotextile-reinforced asphalt is increased by 4.5% and 0.6% compared with unreinforced asphalt, corresponding to AC-13C and AC-20C. Comparing AC-20C and AC-13C asphalt beams, it can be found that the cracking energy of AC-20C asphalt samples are almost the same as the AC-13C asphalt beam. There is little difference between AC-20C and AC-13C samples.

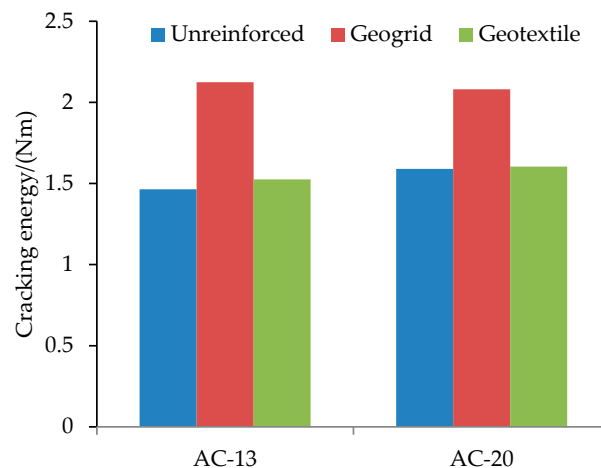


Figure 5. The cracking energy of the six types of asphalt samples.

3.3. Crack Propagation Analyses

Figures 6 and 7 show that only one obvious crack occurs in the beam at a temperature of $-10\text{ }^{\circ}\text{C}$. The crack initiation position is close to the load application point, and the strike is basically perpendicular to the upper and lower surfaces of the beam. The crack opening size of unreinforced asphalt and geotextile-reinforced asphalt was relatively large, while the crack opening size of geogrid-reinforced asphalt was relatively small. When the crack at the bottom of the beam extends to the interlayer, it mainly depends on geosynthetics to inhibit the further expansion of the crack. However, due to the lower tensile strength of the geotextile, the geotextile will be damaged over time, and will finally form a crack with a large opening. The tensile strength of the geogrid is relatively high and will not be damaged, but the geogrid will be deformed to a certain extent. The deformation is really small; however, the asphalt has reached the cracking limit. The crack will continue to expand upward and eventually form a through crack with a small opening.

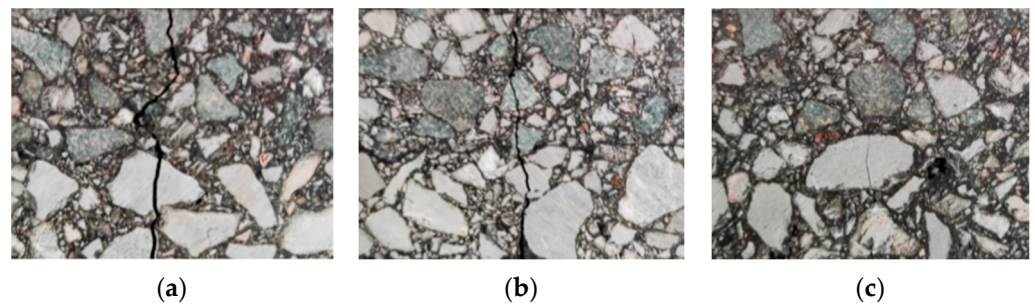


Figure 6. Crack propagation diagram of the AC-13C. (a) Unreinforced, (b) geotextile, (c) geogrid.

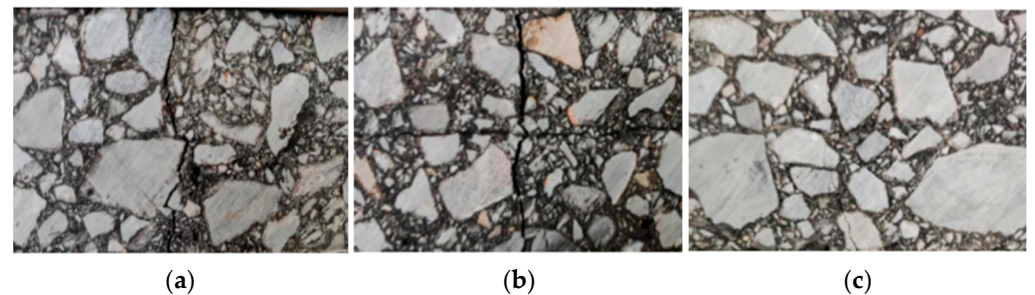


Figure 7. Crack propagation diagram of the AC-20C. (a) Unreinforced, (b) geotextile, (c) geogrid.

4. Conclusions

This article has discussed the cracking resistance behavior of geosynthetics-reinforced asphalt at $-10\text{ }^{\circ}\text{C}$ using the bending test. The following conclusions can be drawn regarding the results presented:

1. Compared with the unreinforced asphalt sample, the flexural tensile strength at failure of the geogrid-reinforced sample was increased by 14.1% and 12.3%, and the geotextile-reinforced sample was reduced by 2.5% and 3.6%, corresponding to AC-13C and AC-20C. The values of the bending stiffness modulus of the geogrid and geotextile-reinforced samples were reduced by 6% and 1%;
2. Through the analysis of the maximum load, flexural tensile strength, and maximum bending tensile strain, it is shown that the cracking resistance behavior of geogrid-reinforced asphalt is better than unreinforced and geotextile-reinforced asphalt at a temperature of $-10\text{ }^{\circ}\text{C}$;
3. The flexural tensile strength at failure of the AC-20C asphalt samples is higher than the AC-13C asphalt samples. The initial deflections of the geogrid and geotextile asphalt layer are higher than the unreinforced sample of the AC-13C. However, the initial deflections of the geogrid and geotextile asphalt layer are lower than the unreinforced

sample for the AC-20C. The reason may be that the maximum aggregate size is different between the AC-20C and the AC-13C;

4. The asphalt shows obvious brittleness at a temperature of $-10\text{ }^{\circ}\text{C}$, and the existence of the geosynthetics does not change the shape of the load–deflection curves. Compared to the previously published results at a temperature of $20\text{ }^{\circ}\text{C}$ or $13\text{ }^{\circ}\text{C}$, geosynthetics have no obvious inhibition effect on crack propagation at a temperature of $-10\text{ }^{\circ}\text{C}$;

5. The cracking energy of the geogrid-reinforced asphalt is 45.2% and 30.8% higher than unreinforced asphalt, corresponding to AC-13C and AC-20C. The cracking energy of the geotextile-reinforced asphalt is increased by 4.5% and 0.6% compared with unreinforced asphalt, corresponding to AC-13C and AC-20C. The cracking energy of AC-20C asphalt samples are almost the same as the AC-13C asphalt samples.

Author Contributions: Conceptualization, Q.L.; formal analysis, Q.L.; investigation, Q.L., P.S. and B.L.; data curation, Q.L., P.S. and B.L.; writing—original draft preparation, Q.L.; writing—review and editing, Y.H. and G.Y.; supervision, Y.H. and G.Y.; project administration, G.Y.; methodology P.S. and B.L.; validation P.S. and B.L. All authors have read and agreed to the published version of the manuscript.

Funding: This research was funded by the Key Research and Development Program of Hebei Province (Grant no. 20375504D).

Institutional Review Board Statement: Not applicable.

Informed Consent Statement: Not applicable.

Data Availability Statement: Not applicable.

Conflicts of Interest: The authors declare no conflict of interest.

Nomenclature

Notations

UN	Unreinforced asphalt
CF	Carbon geogrid-reinforced asphalt
GT	Geotextile-reinforced asphalt
FP	Glass fiber-reinforced polymer geogrid
NR	No-reinforcement asphalt
GF	Reinforced with glass geogrid
R1	Reinforced with continuous fiberglass fabric
R2	Reinforced with a non-woven polyester fabric and multidirectional fiberglass

References

1. Ferrotti, G.; Canestrari, F.; Virgili, A.; Grilli, A. A Strategic Laboratory Approach for the Performance Investigation of Geogrids in Flexible Pavements. *Constr. Build. Mater.* **2011**, *25*, 2343–2348. [[CrossRef](#)]
2. Ferrotti, G.; Canestrari, F.; Pasquini, E.; Virgili, A. Experimental Evaluation of the Influence of Surface Coating on Fiberglass Geogrid Performance in Asphalt Pavements. *Geotext. Geomembranes* **2012**, *34*, 11–18. [[CrossRef](#)]
3. Saride, S.; Kumar, V.V. Influence of Geosynthetic-Interlayers on the Performance of Asphalt Overlays on Pre-Cracked Pavements. *Geotext. Geomembranes* **2017**, *45*, 184–196. [[CrossRef](#)]
4. Lee, J.H.; Baek, S.B.; Lee, K.H.; Kim, J.S.; Jeong, J.H. Long-Term Performance of Fiber-Grid-Reinforced Asphalt Overlay Pavements: A Case Study of Korean National Highways. *J. Traffic Transp. Eng.* **2019**, *6*, 366–382. [[CrossRef](#)]
5. Lee, J.; Kim, Y.R.; Lee, J. Rutting Performance Evaluation of Asphalt Mix with Different Types of Geosynthetics Using MMLS3. *Int. J. Pavement Eng.* **2015**, *16*, 894–905. [[CrossRef](#)]
6. Partl, M.N.; Sokolov, K.; Kim, H. Evaluating and Modelling the Effect of Carbon Fiber Grid Reinforcement in a Model Asphalt Pavement. In Proceedings of the Fourth International Conference on FRP Composites in Civil Engineering (CICE2008), Zurich, Switzerland, 22 July 2008; pp. 22–24.
7. Canestrari, F.; Belogi, L.; Ferrotti, G.; Graziani, A. Shear and Flexural Characterization of Grid-Reinforced Asphalt Pavements and Relation with Field Distress Evolution. *Mater. Struct. Constr.* **2015**, *48*, 959–975. [[CrossRef](#)]
8. Zofka, A.; Maliszewski, M.; Maliszewska, D. Glass and Carbon Geogrid Reinforcement of Asphalt Mixtures. *Road Mater. Pavement Des.* **2017**, *18*, 471–490. [[CrossRef](#)]

9. Ingrassia, L.P.; Virgili, A.; Canestrari, F. Effect of Geocomposite Reinforcement on the Performance of Thin Asphalt Pavements: Accelerated Pavement Testing and Laboratory Analysis. *Case Stud. Constr. Mater.* **2020**, *12*, e00342. [[CrossRef](#)]
10. Ragni, D.; Montillo, T.; Marradi, A.; Canestrari, F. *Fast Falling Weight Accelerated Pavement Testing and Laboratory Analysis of Asphalt Pavements Reinforced with Geocomposites*; Springer International Publishing: New York, NY, USA, 2020; Volume 48, ISBN 9783030297794. [[CrossRef](#)]
11. Kumar, V.V.; Saride, S. Evaluation of Cracking Resistance Potential of Geosynthetic Reinforced Asphalt Overlays Using Direct Tensile Strength Test. *Constr. Build. Mater.* **2018**, *162*, 37–47. [[CrossRef](#)]
12. Spadoni, S.; Ingrassia, L.P.; Paoloni, G.; Virgili, A.; Canestrari, F. Influence of Geocomposite Properties on the Crack Propagation and Interlayer Bonding of Asphalt Pavements. *Materials* **2021**, *14*, 5310. [[CrossRef](#)] [[PubMed](#)]
13. Ram Kumar, B.A.V.; Jallu, H. *Performance of Geogrid Reinforced Asphalt Layers—A Review*; Springer: Singapore, 2022; Volume 172, ISBN 9789811643958.